6th European Conference on Computational Mechanics (ECCM 6)
7th European Conference on Computational Fluid Dynamics (ECFD 7)
1115 June 2018, Glasgow, UK

AERODYNAMIC OPTIMIZATION USING FSI COUPLED ADJOINTS IN SU2

Charanya Venkatesan-Crome[1], Ruben Sanchez[2] and Rafael Palacios[1]

[1] Department of Aeronautics
Imperial College London,
London, SW7 2AZ, United Kingdom
email: charanya.crome09@imperial.ac.uk

[2] Chair for Scientific Computing
TU Kaiserslautern
67663 Kaiserslautern, Germany

Key words: multidisciplinary design optimization, aeroelasticity, algorithmic differentiation, adjoint method

Abstract. This paper discusses the development of the native non-linear fluid-structure interaction solver in the open source SU2 package, along with the coupled adjoint calculations for aeroelastic optimization. A compliant NACA 0012 airfoil test case is investigated with a clamped leading edge and flexibility in the rest of the airfoil as dictated by a varying stiffness distribution. The objective function of aerodynamic efficiency was used, calculated in aeroelastic equilibrium, with structural material properties as the design variables. The sensitivity to the input design variables is calculated through the Algorithmic-Differentiation-based Discrete Adjoint (ADDA) sensitivity analysis method. Aeroelastic optimization using sequential least squares programming is demonstrated for transonic aerodynamics governed by the Euler equations.

1 INTRODUCTION

Aerodynamic optimization has long been studied [1, 2] in order to use Computational Fluid Dynamic (CFD) techniques for not only analysis but also design. These methods consider the external shape, but it is increasingly relevant to take into account the internal structure. This has led to the development of multidisciplinary design optimization (MDO) techniques for wing and aircraft design, which rely on the modelling of fluid-structure interaction (FSI) [3, 4, 5].

The framework for optimization in this work is the open source SU2 package. SU2 is a multi-physics solver for aerodynamic design [6, 7]. Some examples of applications of SU2 include aeroacoustics [8, 9, 10], turbomachinery [11, 12] and aeroelasticity [13, 14]. A native, fully coupled non-linear FSI solver has been built by Sanchez *et al* [13, 14] which will be used in this paper. Adjoint-based optimization provides huge computational advantage for optimization with large number of design variables. This is the case of shape

optimization [15, 1, 2]. However, this methodology often requires manual linearization which becomes increasingly time-consuming with increasing complexity of the problem to be solved. Algorithmic differentiation has been seen to be an efficient alternative to manually-differentiated adjoints. This methodology has been implemented for the fluid solver in SU2 by Albring et al. [16, 17], and later for the fully coupled adjoint FSI solver by Sanchez et al [14].

The paper is organized such that Section 2 briefly presents the governing equations of the FSI primal solver and the adjoint equations. Section 3 discusses the numerical results of the preliminary aeroelastic optimization. Finally, section 4 summarizes the conclusions and future work.

2 BACKGROUND

The fluid-structure interaction problem is defined such that the fluid and structure domains are governed by their own constitutive equations and interact with each other over a common interface. Brief description will be given below, and full description of this implementation can be found in the papers by Sanchez et al [13, 14]. A three-field partitioned approach is used in which along with structure, $\mathscr{S}$, and fluid domain, $\mathscr{F}$, the third field is the mesh, $\mathscr{M}$, which allows the transfer of displacement information in the structure to the fluid domain as required. This type of formulation, though is more computationally expensive than a two-field formulation, has been found to be suitable for problems with large structural displacements [18, 3], therefore is the chosen strategy for this work.

The governing equations of the three-field formulation can be symbolically written as

$$\mathscr{G} = \mathscr{G}(\mathbf{u}, \mathbf{w}, \mathbf{z}) = \begin{cases} \mathscr{S} & = \mathscr{S}(\mathbf{u}, \quad \mathbf{w}, \quad \mathbf{z}) \quad = \mathbf{0} \\ \mathscr{F} & = \mathscr{F}(\qquad \mathbf{w}, \quad \mathbf{z}) \quad = \mathbf{0} \\ \mathscr{M} & = \mathscr{M}(\mathbf{u}, \qquad \mathbf{z}) \quad = \mathbf{0}, \end{cases} \tag{1}$$

where $\mathbf{w}$ is the discrete unknowns on the fluid domain, the discretized nodal positions of the fluid mesh are defined by $\mathbf{z}$ and the discretized nodal displacements of the structure are defined by $\mathbf{u}$. The key features in the solution of each of the three fields are outlined next.

2.1 Fluid Dynamics

The fluid solver in SU2 has been designed for partial differential equations representing numerous flow types on a domain Ω. Here, the fluid problem in (1) is defined using the compressible form of the Navier-Stokes equation for viscous flow,

$$\frac{\partial \mathbf{w}_\Omega}{\partial t} + \nabla \cdot \mathbf{F^c}(\mathbf{w_\Omega}, \mathbf{z_\Omega}) - \nabla \cdot \mathbf{F^v}(\mathbf{w_\Omega}, \mathbf{z_\Omega}) - \mathbf{Q} = 0 \tag{2}$$

where $\mathbf{F^c}$ and $\mathbf{F^v}$ are the convective and viscous fluxes respectively and $\mathbf{Q}$ is a generic source term. For Euler flows, which will be used in this work, $\mathbf{Q}$ and $\mathbf{F^v}$ are zero. The remaining two variables are defined by,

$$\mathbf{w}_\Omega = \{\rho, \rho\mathbf{v}, \rho e\}^\mathsf{T}, \quad \mathbf{F^c} = \left\{ \begin{array}{c} \rho(\mathbf{v} - \dot{\mathbf{z}}_\Omega) \\ \rho\mathbf{v} \otimes (\mathbf{v} - \dot{\mathbf{z}}_\Omega) + \bar{\bar{I}}p \\ \rho e(\mathbf{v} - \dot{\mathbf{z}}_\Omega) + p\mathbf{v} \end{array} \right\} \tag{3}$$

where ρ is the fluid density, $\mathbf{v} = \{v_1, v_2, v_3\}^\mathsf{T} \in \mathbb{R}^3$ is the vector of flow speeds in a Cartesian system of reference, e is the total energy per unit mass and p is the static pressure. The discretized mesh velocity vector at point of evaluation of the flux is defined by $\dot{\mathbf{z}}_\Omega$, however only the equilibrium condition is used for the static cases discussed in this work.

Assuming a perfect gas with a ratio of specific heats γ and gas constant R, the pressure and temperature are given by $p = (\gamma - 1)\rho\left[e - \frac{1}{2}(\mathbf{v} \cdot \mathbf{v})\right]$ and $T = p/(\rho R)$ respectively. The partial differential equations are discretized using a finite volume method on a dual grid with control volumes constructed using a median-dual vertex-based scheme [7]. The convective fluxes can be discretized using centered or upwind schemes in SU2 and for this work the centered Jameson-Schmidt-Turkel (JST) scheme has been used.

2.2 Structural Mechanics

Formulation based on the finite deformation framework of Bonet and Wood [19] has been used to define the structural domain to allow problems with large displacements which are discretized in space using isoparametric finite elements. The pointwise equilibrium condition in the structure, ignoring inertial effects, is defined by

$$\text{div}\ \boldsymbol{\sigma} + \mathbf{f} = \mathbf{0}, \tag{4}$$

where $\boldsymbol{\sigma}$ is the Cauchy stress tensor and $\mathbf{f}$ is the actuating forces per unit volume acting on the structure. A weak form of the equilibrium is obtained through the principle of virtual work. For an arbitrary virtual displacement, $\delta\mathbf{r}$, from a current configuration of the body, the equilibrium condition can be described by

$$\delta\mathbf{W} = \int_v \boldsymbol{\sigma} : \delta\mathbf{d}\ dv - \left(\int_v \mathbf{f} \cdot \delta\mathbf{r}\ dv + \int_{\partial v} \mathbf{t} \cdot \delta\mathbf{r}\ da \right) = \mathbf{0}, \tag{5}$$

where the Cauchy stress tensor $\boldsymbol{\sigma}$ together with the virtual rate of deformation tensor $\mathbf{d}$ defines the internal component of the virtual work. The external component is defined by the sum contributed by both actuating forces per unit volume $\mathbf{f}$, and the applied surface traction per unit area, $\mathbf{t}$. The volume of the body is defined by v and external surface is represented by ∂v.

The equilibrium condition defined by (5) can be discretized to lead to structural field problem of (1), which is defined by

$$\mathscr{S}(\mathbf{u}, \mathbf{w}, \mathbf{z}) = \mathbf{T}(\mathbf{u}) - \mathbf{F}_b - \mathbf{F}_\Gamma(\mathbf{u}, \mathbf{w}, \mathbf{z}) = \mathbf{0}, \tag{6}$$

where $\mathbf{T}(\mathbf{u})$ are the internal equivalent forces, $\mathbf{F}_b$ are the body forces, and $\mathbf{F}_\Gamma(\mathbf{u}, \mathbf{w}, \mathbf{z})$ are the surface forces acting over the boundary Γ.

The constitutive model used in this work assumes isotropic, hyperelastic structure. Neo-Hookean material model [19] is used for which the Cauchy stress tensor is defined as

$$\boldsymbol{\sigma}_{NH} = \frac{\mu}{j}\left(\mathbf{b} - \mathbf{I}\right) + \frac{\lambda}{j}(\ln j)\mathbf{I}, \tag{7}$$
$$\lambda = \frac{E\nu}{(1+\nu)(1-2\nu)} \quad ; \quad \mu = \frac{E}{2(1+\nu)},$$

where j is the determinant of the deformation gradient of the structural problem, $\mathbf{b}$ is the left Cauchy-Green deformation tensor, E is the Young's modulus and ν is the Poisson ratio of the material.

2.3 Mesh Domain

The mesh domain is the third field of the problem, incorporated in order to handle large displacements from the structural mesh which would modify the fluid domain. A pseudo-linear elastic definition is used to describe the mesh domain as

$$\mathscr{M}(\mathbf{u}, \mathbf{z}) = \tilde{\mathbf{K}}_m \mathbf{z} - \tilde{\mathbf{f}}(\mathbf{u}), \tag{8}$$

where $\tilde{\mathbf{K}}_m$ is the fictitious stiffness matrix of the mesh and $\tilde{\mathbf{f}}$ is the fictitious force to enforce matching boundary displacements.

2.4 Coupled Problem

The coupled problem is defined by combining the continuity of displacements over the common interface and the equilibrium conditions for the fluid and structural tractions. A Dirichlet-to-Neumann operator is defined for the fluid domain to map the fluid tractions using the fluid displacements at the fluid-structure interaction boundary, Γ. Similarly, a Neumann-to-Dirichlet operator is defined for the structural domain which maps the structural displacements on the interface using the structural tractions. This enables the following fixed-point iteration:

$$\mathscr{D}_S^{-1}(-\mathscr{D}_F(\mathbf{u}_\Gamma)) = \mathbf{u}_\Gamma. \tag{9}$$

The coupled problem is solved using non-linear Block Gauss-Seidel iterations as described by Barcelos and Maute [20]. In each iteration, the governing equations for the fluid, structure and mesh fields are solved sequentially, and the convergence criterion is evaluated. This criterion corresponds to the residual of displacements at the interface to be within tolerance, $\mathscr{R}_\mathbf{u} = \|\mathbf{u}_\Gamma^{n+1} - \mathbf{u}_\Gamma^n\| < \epsilon$.

To prevent the appearance of divergence issues, a relaxation parameter has been incorporated to the formulation [21, 13]. In addition to this, a ramped loading is used which transfers the loads to the structural domain during a specified number of BGS iterations [13]. This ramp is used to prevent overshoots in the solution process of the first few structural iterations, due to large variations in the external and internal forces balance.

2.5 Fluid-structure interaction adjoint solution using algorithmic differentiation

For an objective function J, the constrained optimization problem can be defined as

$$\begin{aligned} &\min_{\mathbf{a}} J(\mathbf{u}, \mathbf{w}, \mathbf{z}, \mathbf{a})) \\ &\text{subject to } \mathscr{G}(\mathbf{u}, \mathbf{w}, \mathbf{z}, \mathbf{a}) = 0, \end{aligned} \tag{10}$$

where $\mathbf{a}$ is a vector design variables. In particular, in this work $\mathbf{a}$ is a vector of multipliers applied to a reference Young modulus, E_{ref}, on different regions of the structural domain to lead to bespoke Young modulus distribution dictated by $\mathbf{E}$

$$\mathbf{E} = \mathbf{a} \cdot \mathrm{E}_{ref}. \tag{11}$$

The aerodynamic resultant forces are computed by,

$$\mathbf{F} = \int_{\partial v} p\, \mathbf{n}_S \, ds. \tag{12}$$

where p is the static pressure on the boundary surface, S is the boundary surface and $\mathbf{n}_S$ is the unit normal vector. The objective in this work is to maximise efficiency, therefore the cost function, $J = -C_L/C_D$, is used where the lift and drag coefficients are obtained from the rotation of $\mathbf{F}$ with the angle of attack of the problem [22]. Using structural design variables with an aerodynamic goal implies that J is implicitly dependent not only on the structural problem, but also on the fully coupled adjoint solution of a fluid-structure interaction problem, which will be discussed briefly below.

By considering the dependencies of each sub-problem and re-writing the problem in fixed point iterators [14], the overall optimization problem can be obtained. The structural problem depends on the state variables from all three fields and can also be explicitly dependent on the design variables,

$$\mathscr{S}(\mathbf{u}^*, \mathbf{z}^*, \mathbf{w}^*, \mathbf{a}) = \mathbf{0} \Leftrightarrow \mathbf{u}^* = \mathbf{S}(\mathbf{u}^*, \mathbf{z}^*, \mathbf{w}^*, \mathbf{a}), \tag{13}$$

where * refers to the variables at which the solution to the fixed-point operator is feasible.

The flow problem depends explicitly on its own conservative variables and on the position of the nodes on the flow domain (including the FSI interface), but the dependence on the structural state variables is not direct due to the three-field formulation. For completeness, explicitly dependent design variables for the flow solver are also included:

$$\mathscr{F}(\mathbf{w}^*, \mathbf{z}^*, \mathbf{a}) = \mathbf{0} \Leftrightarrow \mathbf{w}^* = \mathbf{G}(\mathbf{w}^*, \mathbf{z}^*, \mathbf{a}). \tag{14}$$

The mesh problem is dependent on the structural domain and possibly on the design variables:

$$\mathscr{M}(\mathbf{u}^*, \mathbf{z}^*) = \mathbf{0} \Leftrightarrow \mathbf{z}^* = \mathbf{M}(\mathbf{u}^*, \mathbf{a}). \tag{15}$$

Therefore, the overall constrained optimization problem is represented by

$$\begin{aligned} \min \quad & J(\mathbf{w}(\mathbf{a}), \mathbf{z}(\mathbf{a}), \mathbf{u}(\mathbf{a}), \mathbf{a}) \\ \text{subject to} \quad & \mathbf{u}(\mathbf{a}) = \mathbf{S}(\mathbf{u}(\mathbf{a}), \mathbf{w}(\mathbf{a}), \mathbf{z}(\mathbf{a}), \mathbf{a}) \\ & \mathbf{w}(\mathbf{a}) = \mathbf{G}(\mathbf{w}(\mathbf{a}), \mathbf{z}(\mathbf{a}), \mathbf{a}) \\ & \mathbf{a}(\mathbf{a}) = \mathbf{M}(\mathbf{u}(\mathbf{a}), \mathbf{a}). \end{aligned} \tag{16}$$

By defining the Lagrangian of the coupled problem, the gradient of the objective function with respect to the design variables can be described using the adjoint variables as

$$\frac{\mathrm{d}J}{\mathrm{d}\mathbf{a}} = \frac{\partial J}{\partial \mathbf{a}} + \bar{\mathbf{u}}^T \frac{\partial \mathbf{S}}{\partial \mathbf{a}} + \bar{\mathbf{w}}^T \frac{\partial \mathbf{G}}{\partial \mathbf{a}} + \bar{\mathbf{z}}^T \frac{\partial \mathbf{M}}{\partial \mathbf{a}}. \tag{17}$$

Differentiating the Lagrangian with respect to the structural variables $\mathbf{u}$, the flow conservative variables $\mathbf{w}$, and the mesh variables $\mathbf{z}$, leads to the implicit adjoint equations which can be written in fixed-point iterators as

$$\bar{\mathbf{x}}^{n+1} = \tilde{\mathscr{G}}(\bar{\mathbf{x}}^n) \Leftrightarrow \begin{cases} \bar{\mathbf{u}}^{n+1} & = \tilde{\mathbf{S}}(\bar{\mathbf{u}}^n, \bar{\mathbf{u}}_{\bar{\mathbf{z}}}) & = \frac{\partial J}{\partial \mathbf{u}}^T + \frac{\partial \mathbf{S}}{\partial \mathbf{u}}^T \bar{\mathbf{u}}^n + \bar{\mathbf{u}}_{\bar{\mathbf{z}}}, \\ \bar{\mathbf{w}}^{n+1} & = \tilde{\mathbf{G}}(\bar{\mathbf{w}}^n, \bar{\mathbf{w}}_{\bar{\mathbf{u}}}) & = \frac{\partial J}{\partial \mathbf{w}}^T + \frac{\partial \mathbf{G}}{\partial \mathbf{w}}^T \bar{\mathbf{w}}^n + \bar{\mathbf{w}}_{\bar{\mathbf{u}}}, \\ \bar{\mathbf{z}} & = \tilde{\mathbf{M}}(\bar{\mathbf{z}}_{\bar{\mathbf{u}}}, \bar{\mathbf{z}}_{\bar{\mathbf{w}}}) & = \frac{\partial J}{\partial \mathbf{z}}^T + \bar{\mathbf{z}}_{\bar{\mathbf{u}}} + \bar{\mathbf{z}}_{\bar{\mathbf{w}}}, \end{cases} \tag{18}$$

with the cross-dependencies defined by

$$\bar{\mathbf{w}}_{\bar{\mathbf{u}}}^T = \bar{\mathbf{u}}^T \frac{\partial \mathbf{S}}{\partial \mathbf{w}} \;\; ; \quad \bar{\mathbf{u}}_{\bar{\mathbf{z}}}^T = \bar{\mathbf{z}}^T \frac{\partial \mathbf{M}}{\partial \mathbf{u}} \;\; ; \quad \bar{\mathbf{z}}_{\bar{\mathbf{w}}}^T = \bar{\mathbf{w}}^T \frac{\partial \mathbf{G}}{\partial \mathbf{z}} \;\; ; \quad \bar{\mathbf{z}}_{\bar{\mathbf{u}}}^T = \bar{\mathbf{u}}^T \frac{\partial \mathbf{S}}{\partial \mathbf{z}}, \tag{19}$$

A BGS routine similar to the primal described earlier, as proposed by Martins [23] and Barcelos [20], is used to find the solution to the coupled adjoint problem. The adjoint variables are calculated using the reverse mode of algorithmic differentiation.

The process begins with a converged solution that is registered as the input. Following one solver iteration, the objective function is registered in the appropriate governing equation iteration. The adjoint variable from this iteration is registered as the output which is used to initialize the adjoint for the next iteration. The algorithm performs a reverse run through the recorded path of the governing equations and extracts the new adjoint output. The algorithm loops through the routine until the the adjoint residual is within tolerance, or alternatively until a maximum number iterations are reached.

For the optimization, the objective function and gradient evaluated above will be used by sequential least-squares programming (SLSQP) optimizer available in SciPy, to update the design variable within user-defined bounds for each iteration [24].

3 NUMERICAL RESULTS AND DISCUSSION

In this section, the aeroelastic optimization described above will be demonstrated for a compliant NACA 0012 aerofoil, with results restricted to small displacements at this stage. The optimization aims to maximize aerodynamic efficiency through the modification of the stiffness distribution. Figure 1 illustrates the computational domain of the fluid

and structural mesh. The chord length of the airfoil, c, was 1 m, and a farfield of 20 chord lengths was used to ensure freestream boundary conditions were captured. The airfoil was clamped at the leading edge up to 20% chord, while the rest of the structure was characterized by a distribution of stiffness split into 10 regions on the upper and lower halves as shown in Figure 1. Thus, there are a total of 20 design variables for the optimization problem, as described in (11). The freestream conditions and the structural properties are defined in Table 1.

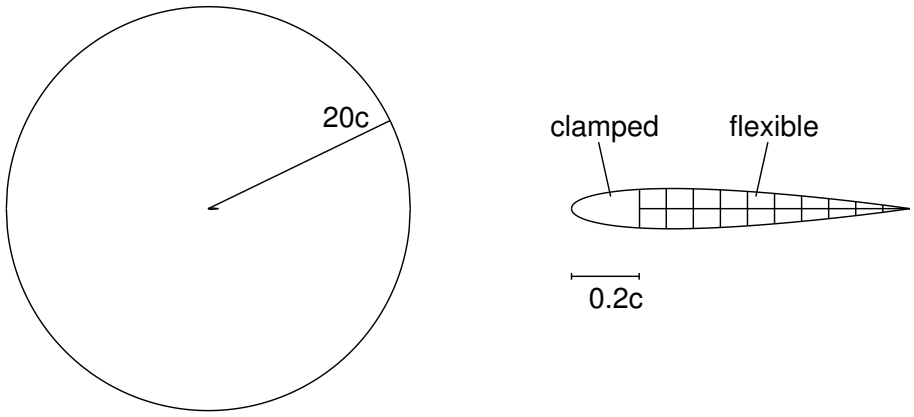

Figure 1: Problem description of the fluid and structural domain

Table 1: Freestream conditions and structural properties for the FSI problem

Mach Number, Ma	0.8	Fluid Density, ρ_f	1.18 kg/m^3
Angle of Attack, α	1.0 °	Airfoil Density, ρ_s	8000 kg/m^3
Pressure, p_{dyn}	0.355 Pa	Poisson Ratio, ν	0.4
Temperature, T_∞	0.002 K	Young Modulus, E_{ref}	20 kPa

3.1 Convergence Study

Mesh convergence study was carried out on both the fluid and structural mesh to ensure suitability for this work. Since the displacements involved are restricted to be small, this study was carried out independently on the two domains, albeit the coupled simulation. Firstly, for the fluid domain three meshes were tested the results of which are shown in Figure 2 (a). Moving from the coarse mesh to the medium fine caused 2.6% variation in efficiency but further refinement beyond the medium mesh only yielded variation of 0.2%. Therefore, the medium fine mesh was chosen for the fluid mesh which had 5233 nodes and 10216 triangular elements.

For the structural domain, the results from five meshes are shown in Figure 2 (b). The first refinement from the coarse mesh led to change in tip displacement of 4.3%. Further

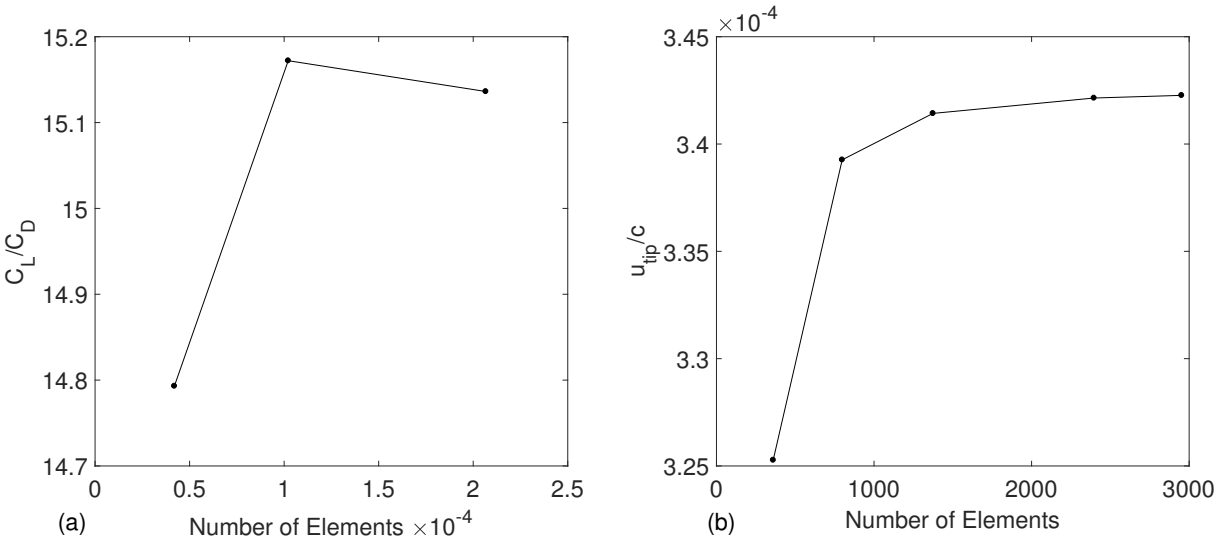

Figure 2: Mesh Independence (a) Flow mesh (b) Structural mesh

refinements had less effect leading to a total of only 0.9% variation but increased the computational cost by over three times. Therefore the second mesh was chosen for the structural domain, which had 795 nodes, 158 triangular elements and 640 quadrilateral elements.

3.2 Aerodynamic Optimization using Stiffness Distribution

An unconstrained aerodynamic optimization was set-up, with the design variables bounded between 0.1 to 10 to keep the structural displacements small. Figure 3 (a) shows the evolution of the objective function during the iterations starting from $k_j = 1$ for $j = 1, 10, 16, 40$. Around 20 iterations are needed for convergence. Figure 3(b) shows the resulting pressure coefficient, C_P, distribution at some of the key iterations. From this it can be seen that there is little change on the upper surface and on the lower surface, the optimizer has slightly delayed the shock formation.

The evolution of the design variables and the structural displacements are shown in Figure 4. For the upper half of the airfoil, the optimization results have led to decreased stiffness prior to the shock, with the design variables being bounded by the lowest permissible value of 0.1 in this region by Iteration 16. In the region beyond of the shock, the gradients have led to the stiffening of the structure.

The lower half followed the same trend of decreased stiffness close to the clamped edge but with increasing stiffness post the shock. The final geometry for the lower half has shown strong sensitivities at the tip and at the region corresponding to the shock on the upper surface with reduced stiffness elsewhere.

Due to the positioning of the stiffness reinforcements and softening of the structure towards the clamped edge, the overall displacement is higher than the equilibrium displacement of the initial design. Figure 4 (d) highlights the difference in resulting shape of the aerofoil beginning with the undeformed NACA0012 ($C_L/C_D = 15.17$) and the de-

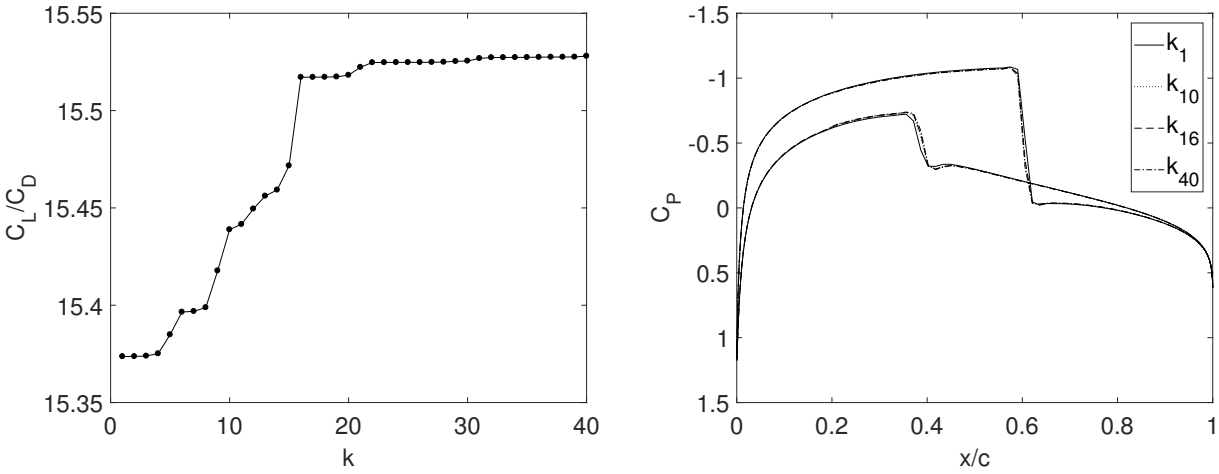

Figure 3: Optimization history: (a) Objective Function (b) C_P distribution from four iterations

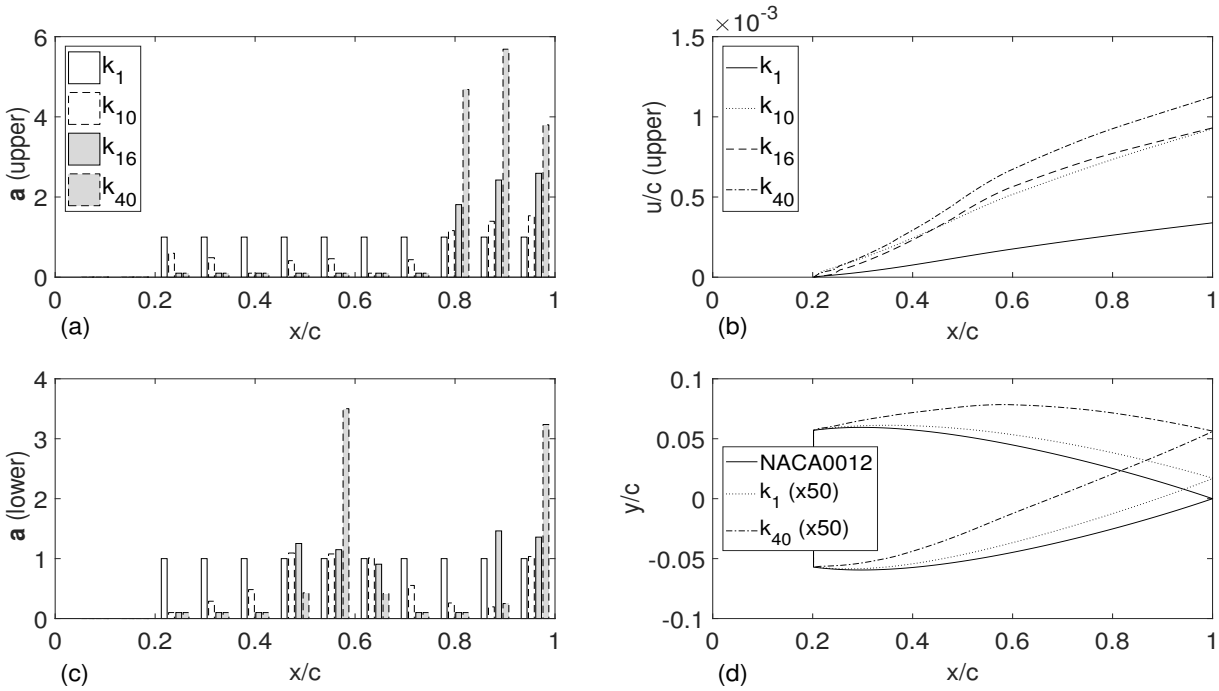

Figure 4: Evolution of design variables on the (a) upper and (c) lower airfoil surfaces, (b) displacement on the upper surface and (d) overall airfoil shapes with deformed shape magnified by $\times 50$

formed shapes magnified by $\times 50$. The initial uniform stiffness distribution led to the upward movement of the airfoil due to the pressure delta created by stronger shock on the suction side. This deformation led to higher aerodynamic efficiency ($C_L/C_D = 15.37$) than the undeformed shape. The optimizer pushed this trend further which led to the optimized deformation with $C_L/C_D = 15.53$ based on the bounded design variables.

4 CONCLUSION

In this paper a framework for aerodynamic optimization using the fully-coupled FSI primal and adjoint solvers in SU2 has been discussed. The framework has been successfully demonstrated using an example of a compliant NACA 0012 airfoil in transonic Euler flow regime, with the aerodynamic efficiency as the objective to maximize and the stiffness distribution in the airfoil as the design parameter. Future work includes the expansion of application to cases with large displacements, and incorporating turbulent effects via the Reynolds Averaged Navier-Stokes equations.

REFERENCES

[1] A. Jameson, "Aerodynamic design via control theory," *Journal of Scientific Computing*, vol. 3, no. 3, pp. 233–260, 1988.

[2] A. Jameson and J. Reuther, "Control theory based airfoil design using the Euler equations," in *5th Symposium on Multidisciplinary Analysis and Optimization*, (Panama City Beach, FL), 1994.

[3] G. K. W. Kenway, G. J. Kennedy, and J. R. R. A. Martins, "Scalable Parallel Approach for High-Fidelity Steady-State Aeroelastic Analysis and Adjoint Derivative Computations," *AIAA Journal*, vol. 52, no. 5, pp. 935–951, 2014.

[4] K. Maute, M. Nikbay, and C. Farhat, "Analytically based sensitivity analysis and optimization of nonlinear aeroelastic systems," in *8th AIAA/USAF/NASA/ISSMO Symposium on Multidisciplinary Analysis and Optimization*, (Long Beach, CA), 2000.

[5] K. Maute, M. Nikbay, and C. Farhat, "Coupled Analytical Sensitivity Analysis and Optimization of Three-Dimensional Nonlinear Aeroelastic Systems," *AIAA Journal*, vol. 39, no. 11, pp. 2051–2061, 2001.

[6] F. Palacios, M. R. Colonno, A. C. Aranake, A. Campos, S. R. Copeland, T. D. Economon, A. K. Lonkar, T. W. Lukaczyk, T. W. R. Taylor, and J. J. Alonso, "Stanford University Unstructured (SU2): An open-source integrated computational environment for multi-physics simulation and design," in *51st AIAA Aerospace Sciences Meeting*, (Grapevine, TX), 2013.

[7] T. D. Economon, F. Palacios, S. R. Copeland, T. W. Lukaczyk, and J. J. Alonso, "SU2: An Open-Source Suite for Multiphysics Simulation and Design," *AIAA Journal*, vol. 54, no. 3, pp. 828–846, 2016.

[8] B. Y. Zhou, T. A. Albring, N. R. Gauger, T. D. Economon, F. Palacios, and J. J. Alonso, "A Discrete Adjoint Framework for Unsteady Aerodynamic and Aeroacoustic Optimization," in *16th AIAA/ISSMO Multidisciplinary Analysis and Optimization Conference*, (Dallas, TX), 2015.

[9] B. Y. Zhou, T. Albring, N. R. Gauger, C. R. Ilario da Silva, T. D. Economon, and J. J. Alonso, "A Discrete Adjoint Approach for Jet-Flap Interaction Noise Reduction," in *58th AIAA/ASCE/AHS/ASC Structures, Structural Dynamics, and Materials Conference*, (Grapevine, TX), 2017.

[10] B. Zhou, T. A. Albring, N. R. Gauger, C. Ilario, T. D. Economon, and J. J. Alonso, "Reduction of Airframe Noise Components Using a Discrete Adjoint Approach," in *18th AIAA/ISSMO Multidisciplinary Analysis and Optimization Conference*, (Denver, CO), pp. 5–9, 2017.

[11] J. A. Keep, S. Vitale, M. Pini, and M. Burigana, "Preliminary verification of the open-source CFD solver SU2 for radial-inflow turbine applications," *Energy Procedia*, vol. 129, pp. 1071–1077, 2017.

[12] M. Pini, G. Persico, D. Pasquale, and S. Rebay, "Adjoint Method for Shape Optimization in Real-Gas Flow Applications," *Journal of Engineering for Gas Turbines and Power*, vol. 137, no. 3, p. 032604, 2014.

[13] R. Sanchez, R. Palacios, T. D. Economon, H. L. Kline, J. J. Alonso, and F. Palacios, "Towards a Fluid-Structure Interaction Solver for Problems with Large Deformations Within the Open-Source SU2 Suite," in *57th AIAA/ASCE/AHS/ASC Structures, Structural Dynamics, and Materials Conference*, (San Diego, CA), 2016.

[14] R. Sanchez, T. Albring, R. Palacios, N. R. Gauger, T. D. Economon, and J. J. Alonso, "Coupled adjoint-based sensitivities in large-displacement fluid-structure interaction using algorithmic differentiation," *International Journal for Numerical Methods in Engineering*, vol. 113, no. 7, pp. 1081–1107, 2018.

[15] J. R. Martins and J. T. Hwang, "Review and Unification of Methods for Computing Derivatives of Multidisciplinary Computational Models," *AIAA Journal*, vol. 51, no. 11, pp. 2582–2599, 2013.

[16] T. Albring, M. Sagebaum, and N. Gauger, "Development of a consistent discrete adjoint solver in an evolving aerodynamic design framework," in *16th AIAA/ISSMO Multidisciplinary Analysis and Optimization Conference*, (Dallas, TX), 2015.

[17] T. Albring, M. Sagebaum, and N. R. Gauger, "Efficient Aerodynamic Design using the Discrete Adjoint Method in SU2," in *17th AIAA/ISSMO Multidisciplinary Analysis and Optimization Conference*, (Washington, DC), 2016.

[18] K. Maute, M. Nikbay, and C. Farhat, "Sensitivity analysis and design optimization of three-dimensional non-linear aeroelastic systems by the adjoint method," *International Journal for Numerical Methods in Engineering*, vol. 56, no. 6, pp. 911–933, 2003.

[19] J. Bonet and R. D. Wood, *Nonlinear Continuum Mechanics for Finite Element Analysis*. Cambridge University Press, 2nd ed., 2008.

[20] M. Barcelos and K. Maute, "Aeroelastic design optimization for laminar and turbulent flows," *Computer Methods in Applied Mechanics and Engineering*, vol. 197, no. 19-20, pp. 1813–1832, 2008.

[21] U. Küttler and W. A. Wall, "Fixed-point fluid-structure interaction solvers with dynamic relaxation," *Computational Mechanics*, vol. 43, no. 1, pp. 61–72, 2008.

[22] T. D. Economon, F. Palacios, and J. J. Alonso, "Unsteady Aerodynamic Design on Unstructured Meshes with Sliding Interfaces," in *51st AIAA Aerospace Sciences Meeting*, (Grapevine, TX), 2013.

[23] J. R. Martins, J. J. Alonso, and J. J. Reuther, "A coupled-adjoint sensitivity analysis method for high-fidelity aero-structural design," *Optimization and Engineering*, vol. 6, no. 1, pp. 33–62, 2005.

[24] E. Jones, T. Oliphant, P. Peterson, *et al.*, "SciPy: Open source scientific tools for Python," 2001–. http://www.scipy.org, [Online; accessed June 2017].